

Article

Petrographic and Geochemical Analysis of Indus Sediments: Implications for Placer Gold Deposits, Peshawar Basin, NW Himalaya, Pakistan

Abdul Mateen ¹, Ali Wahid ^{1,*} , Hammad Tariq Janjuhah ^{2,*} , Muhammad Saleem Mughal ¹, Syed Haroon Ali ³, Numair Ahmed Siddiqui ⁴, Munib Ahmed Shafique ⁵, Olga Koumoutsakou ⁶ and George Kontakiotis ⁶ 

¹ Institute of Geology, University of Azad Jammu and Kashmir, Muzaffarabad 13100, Pakistan

² Department of Geology, Shaheed Benazir Bhutto University Sheringal, Sheringal 18000, Pakistan

³ Department of Earth Sciences, University of Sargodha, Sargodha 40100, Pakistan

⁴ Geosciences Department, Universiti Teknologi PETRONAS, Seri Iskandar 31750, Perak Darul Ridzuan, Malaysia

⁵ Pakistan Institute of Nuclear Science and Technology (PINSTECH), Islamabad 45650, Pakistan

⁶ Department of Historical Geology-Paleontology, Faculty of Geology and Geoenvironment, School of Earth Sciences, National and Kapodistrian University of Athens, Panepistimiopolis, Zografou, 15784 Athens, Greece

* Correspondence: ali.wahid@ajku.edu.pk (A.W.); hammad@sbbu.edu.pk (H.T.J.)



Citation: Mateen, A.; Wahid, A.; Janjuhah, H.T.; Mughal, M.S.; Ali, S.H.; Siddiqui, N.A.; Shafique, M.A.; Koumoutsakou, O.; Kontakiotis, G. Petrographic and Geochemical Analysis of Indus Sediments: Implications for Placer Gold Deposits, Peshawar Basin, NW Himalaya, Pakistan. *Minerals* **2022**, *12*, 1059. <https://doi.org/10.3390/min12081059>

Academic Editors: Vasilios Melfos, Panagiotis Voudouris and Grigorios Aarne Sakellaris

Received: 26 July 2022

Accepted: 19 August 2022

Published: 22 August 2022

Publisher's Note: MDPI stays neutral with regard to jurisdictional claims in published maps and institutional affiliations.



Copyright: © 2022 by the authors. Licensee MDPI, Basel, Switzerland. This article is an open access article distributed under the terms and conditions of the Creative Commons Attribution (CC BY) license (<https://creativecommons.org/licenses/by/4.0/>).

Abstract: Alluvial placer gold deposits that accumulate in streams across the globe are essentially allochthonous sedimentary deposits that are transported from their source to their location of deposition. The purpose of this study was to find placer gold deposits in alluvial sediments along the Indus River in the NW Himalaya of Pakistan. The investigated region was divided into five clusters based on river morphology. The research focused on mineralogical distribution, sediment source, gold transport distance, elemental composition, and gold concentration in river sediments. Throughout, during the deposition at point and channel bars, the mixed source of alluvial sediments was revealed by its mineralogical composition. However, the SEM analysis demonstrated that the gold grains had a high flatness index, indicating that they had been transported a significant distance. The elemental composition of several samples revealed a significant concentration of silicon dioxide, iron oxide, and alumina oxide transported from the Himalaya. The study of the trace elements indicated gold and related base metals with granitic provenance were transported from an acidic/granitic source. Based on gold concentration, it is demonstrated that the left riverbank (clusters C1, C2, and C3) has a higher concentration of gold deposits and higher potential for economic gold exploration than the right bank (clusters C4 and C5) due to the lower velocity of running water in the study area. The findings revealed that the studied area has good potential for commercial exploration of gold resources, and the workflow can be adopted in any region with a similar geological setting and morphology.

Keywords: placer gold deposits; Indus River; petrology; flatness index; geochemistry; trace elements; environmental monitoring; economic mineral deposits

1. Introduction

Gold is one of the most valuable minerals on the planet, consisting mostly of elemental gold with traces of mercury, silver, copper, iron, nickel, manganese, and tinier amounts of selenium, platinum-group metals, bismuth, and rhenium [1–5]. When the gold is about 4 g/ton with other accumulated deposits, it is included in mineral deposits [6]. Placer gold is a type of allochthonous sedimentary deposit that mostly accumulates along shallow streams and rivers with other heavy minerals [7,8]. Mineralogy, morphology, elemental composition, and concentration of trace elements within placers are all debatable studies for the exploration of economic gold resources. This analysis aided in the identification of gold mineralization, prospective source rock, major oxides associated with gold, and concentration of economic gold deposits [9–13]. Moreover, since the accumulation of economic

gold deposits is largely reliant on morphological characteristics, distinct clusters may be identified. As they influence the flow of water, features such as canyon exits, waterfalls, and point bars may change its accumulation in the same place. The aforementioned characteristics substantially reduce water velocity and may be good places for the deposition of heavy minerals, such as gold grains [5].

Gold exploration in the NW Himalaya along the Indus River has been ongoing for a long time [9]. Over the past several decades, national and international organizations have boosted their exploration operations to investigate economic minerals. In 1992–1995, the Gold Exploration and Mineral Analysis Project (GEMAP) undertook commercial mineral investigations, mostly for gold, as part of the Australian Aid for International Development [9]. The aim of this project was to focus on gold and associated minerals in the NW Himalaya. Moreover, many investigations in this region indicate the possibility of gold occurrences eroded from their source rocks [14–17].

The study area is located in the eastern Peshawar Basin of the NW Himalaya, where alluvial sediments of the Indus River are being investigated. Reconnaissance surveys and earlier geological investigations in several areas of the Peshawar Basin have shown the presence of heavy minerals, including gold (Au), in river deposits [18–21]. However, there are no detailed studies available on petrographic, geochemical, or spatial distribution models based on geochemical analysis. Similarly, the identification of economic Au in possible areas of the river environment has not previously occurred. The objectives of this research were to determine the mineralogical and elemental compositions of the alluvial sand deposits in order to understand their possible source and chemical composition. Further, the morphology of alluvial gold is determined based on its internal structure and deposition pattern. The placer gold deposits and the associated trace elements with them are also analyzed in order to determine the economic potential of gold deposits. Finally, a model was developed to identify potential areas for profitable investigation of placer gold deposits.

2. Regional Geology

The Himalaya are the result of the continuous collision of the Indian and Eurasian plates. The Kohistan Island Arc (KIA) is a Cretaceous-era intraoceanic island arc that has been situated between these two plates [22]. The Eurasian plate is separated from the KIA by the Main Karakoram Thrust (MKT), also known as the Shyoke Suture Zone (SSZ) (Figure 1). The Indian Plate and KIA are separated by the Indus-Tsangpo Suture Zone (ITSZ), a major tectonic boundary. The KIA is divided into three parts: the northern and western parts (volcanics and metasediments), the central part (batholith), and the southern part (e.g., contains three tectono-metamorphic units: the Chilas Complex, Kamila Amphibolite, and Jijal Complex). The Himalaya extend about 2000 km in length and are further subdivided into the Greater Himalaya (GH), Lesser Himalaya (LH), and Tethyan Himalaya (TH) [22,23]. The Main Central Thrust (MCT) separates the high-grade crystalline rocks of the GH from the low-grade crystalline rocks of the LH. However, in the west Himalaya, the Zaskar Shear Zone (ZSZ), also known as the South Tibetan Detachment (STD) fault, is present. The Main Boundary Thrust (MBT) separates the LH from the Sub-Himalayan/Himalayan Foreland Basin [24]. The area consists of vast networks of tributaries connected to rivers that run through the Himalaya and impact sediment erosion, transport, and deposition over a long distance (Figure 1). Economic heavy minerals are also transported and deposited along the adjacent areas of these rivers. The Indus River is the main river in the NW Himalaya, rising from GH tributaries including the Hunza, Ghizar, Gilgit, Shyok, and Shigar rivers [10]. The Hunza River originates from the Karakoram through different lithological units, mainly Permian and Triassic limestone and Hunza plutons. It enters the KIA after passing through the Kohistan Batholith (KB). Further, the river enters the metasedimentary rocks of the Gilgit complex by joining the Ghizar River, also known as the Gilgit River. From there on, the Gilgit River connects to the Indus River and flows into the KB. Both the Shyok River, which starts in the SSZ, and Astor River,

that rises in the Deosai Mountains, flow from the KB and join the Shigar River before joining the Indus River in the KIA. The Indus River flows mostly parallel to the strike of KIA. After passing through the Main Mantle Thrust (MMT), it eventually enters the Indian Plate's Besham Basement Complex (BBC) and flows through the Indian Plate rocks. The BBC consists of heterogeneous gneisses, quartzofeldspathic gneisses, amphibolites, granodiorites, pegmatites, quartzite, metacarbonate sedimentary rocks, and leucocratic granites [25].

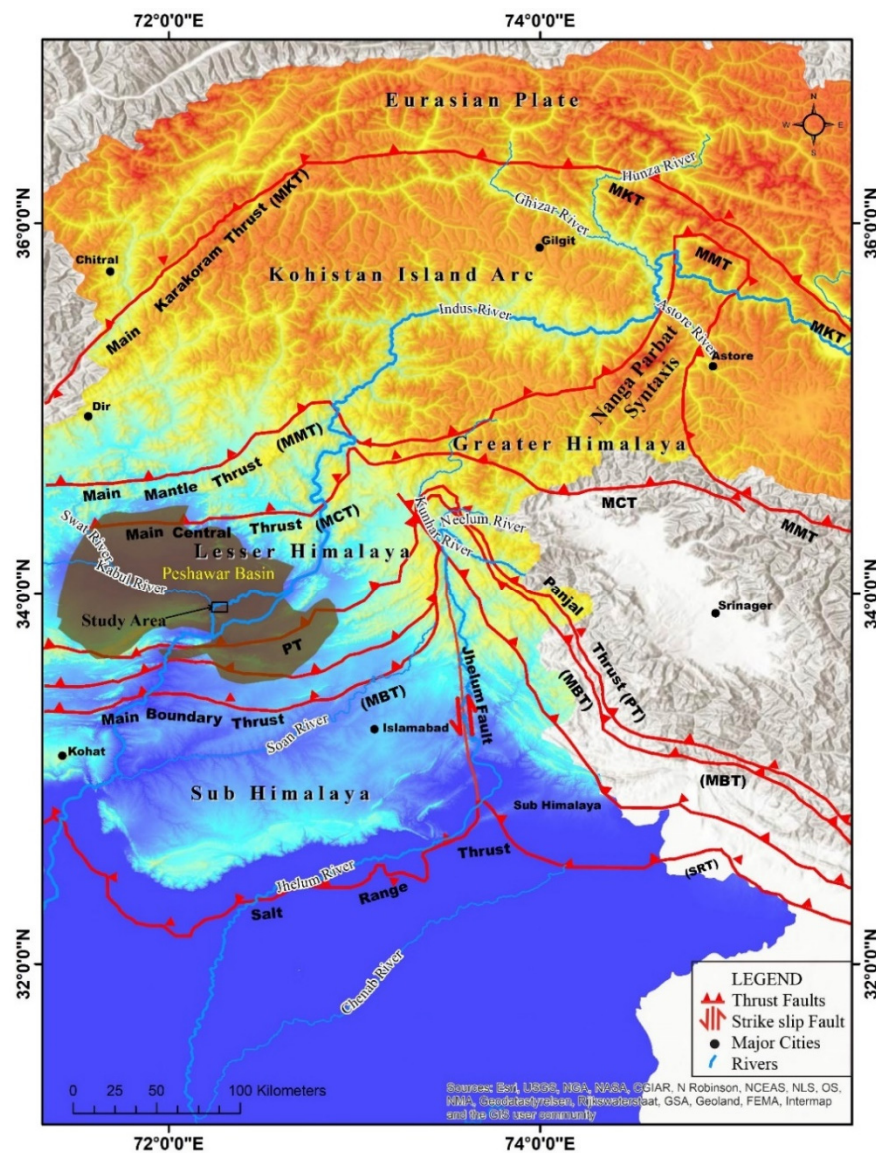


Figure 1. The regional tectonic map of Himalaya indicating the Peshawar basin and the major rivers flowing from the Himalaya to the study area, modified after [24,26,27].

The Peshawar Basin is an intermontane basin located on the Indian Plate in the LH, along the southern edge of the Pakistan Himalaya [5,23]. This intermontane basin originated in the Plio-Pleistocene during the late stages of orogenic episodes caused by Indian–Eurasian plate collisions [24,28,29]. It is responsible for the sediment accumulation in the Attock–Cherat Range and causes pounding drainage [28]. Exposed igneous and metamorphic rocks eroded from northern Pakistan have the potential to provide primary gold in the Himalaya that can be deposited mostly via river systems [5]. These depositions may consist of scattered economic gold clusters deposited by gravity settling [29,30].

The Indus River flows through the Peshawar Basin of the NW Himalaya in the study region, passing through the Alkaline Igneous Province of the Peshawar Plain and unconsolidated sands, silt, and loess of Quaternary age. The basin is bounded by the Attock-Cherat Range to the south, the Gandghan Range to the east, and the Khyber Range to the west (Figure 2a). These ranges comprise metasediments from the Himalaya as well as unmetamorphosed sediments from the GH's Kohat-Potwar plateau [21,31]. The Peshawar Basin is composed of sedimentary fold-and-thrust belts to the south and metamorphic terrains to the north [32]. The Peshawar Basin lithostratigraphy is composed of lithological units ranging from the Precambrian to the Quaternary (Figure 2b). Precambrian formations include the Dakhner Formation, Manki Formation, and Shakhot Formation. The Paleozoic age comprises the Ambar Formation, Misri Formation, Panjpir Formation, and Nowshera Formation [5]. The Peshawar Basin sediments are mostly lacustrine silt, river sand, and gravel [33]. The Quaternary deposits of the Peshawar Basin are mainly composed of alluvial fans, flood plains, lacustrine, deltaic, fluvial, and loess deposits. Pleistocene lakes within the Peshawar Basin are responsible for the presence of parallel bedded, fining upward sand layers, silts, and clays [34].

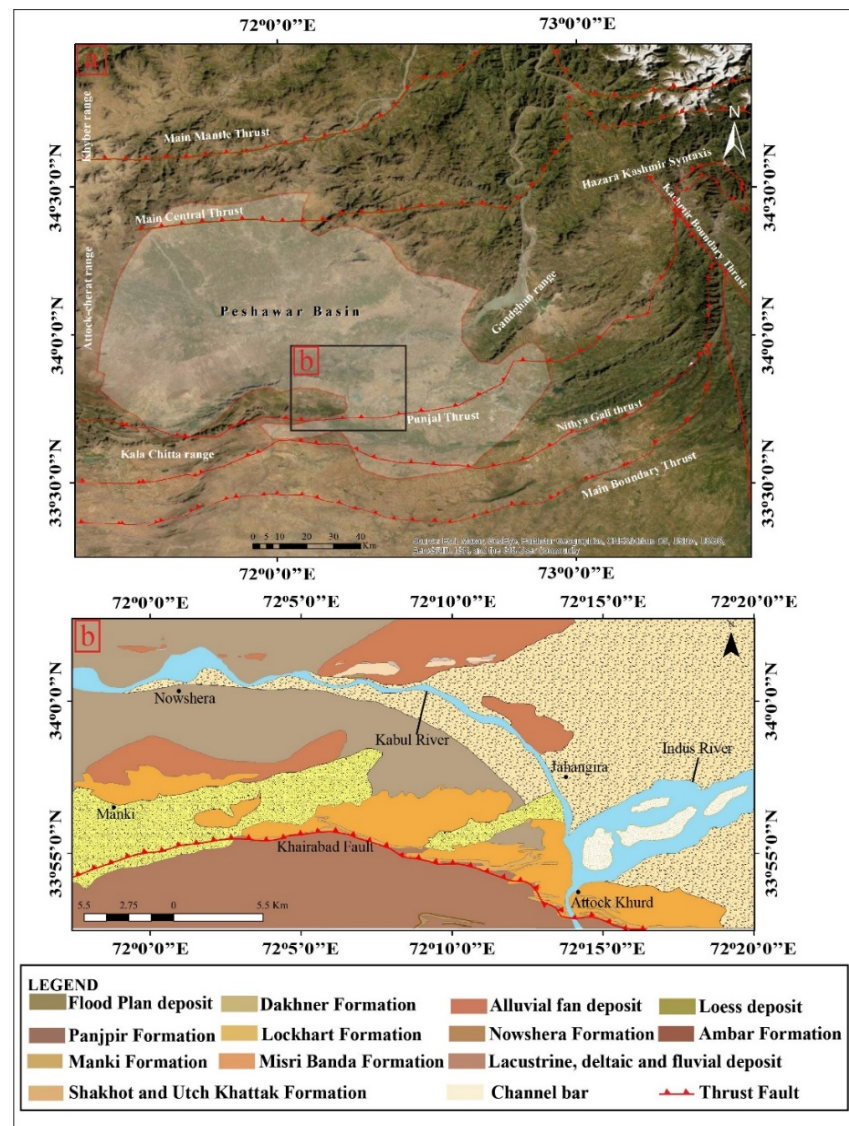


Figure 2. (a) The tectonic features and (b) the lithostratigraphic units of the Peshawar Basin modified after [5,35].

3. Materials and Methods

Based on river morphology, the study region is divided into five clusters, including Attcock-Khurd, Mula Mansoor, Kund, and Allah Dher (Figure 3b). The river morphology was mainly focused on midpoint bars and the inner side of meandering, because they are suitable areas for placer gold deposits. The sedimentary deposits in the study area are mostly composed of river channels and point bars with sand to clay-sized particles found in a finning upward sequence. The various sizes were determined in the field by observing the grittiness of the rocks. From each cluster along the Indus River, we obtained a total of 25 samples. After removing organic content by hand picking, about 8–20 kg of material was collected from a 1 m depth for each sample. The samples were subsequently taken to the riverbank for panning. Further, the heavy mineral concentrations in the samples were collected from the field by refining through sieving and panning to decrease the volume and weight (100–200 g). The samples were named based on their cluster design and collection from the field (Figure 3b).

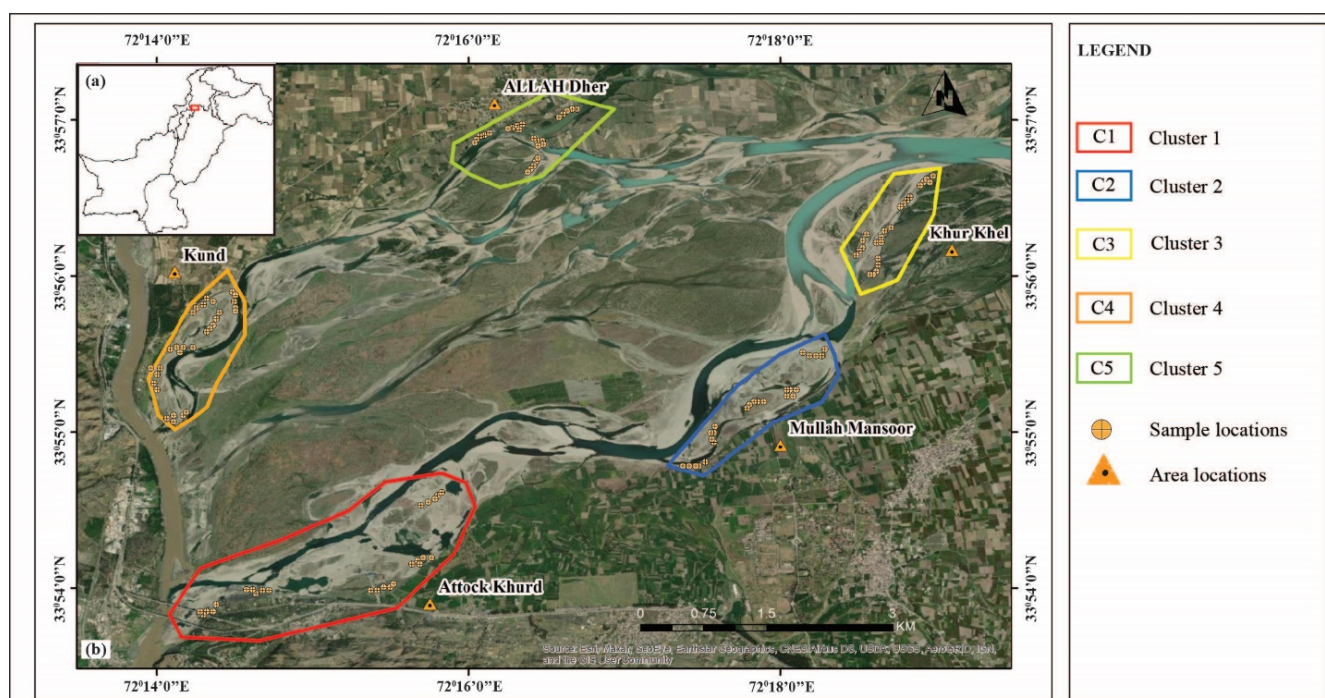


Figure 3. (a) Pakistan location map highlighting the red box of study area, (b) The different clusters were designed based on river morphology for sample collection along the Indus River.

Further, the samples were studied using a stereoscope (Bioveopeak Inc., Seattle, WA, USA), and gold granules were recovered for scanning electron microscopy (SEM, at University of Azad Jammu and Kashmir, Pakistan) analysis to study the morphology of the grains. Representative samples from each cluster, on the other hand, were processed into thin sections and then powdered for X-ray fluorescence spectroscopy (XRF at Centralized Resources Laboratory, University of Peshawar, Pakistan.) and atomic adsorption spectroscopy (AAS at Centralized Resources Laboratory, University of Peshawar, Pakistan) analysis to identify the mineralogical composition, elemental compositions, and quantity of gold in the studied samples, respectively. inductively coupled plasma–atomic emission spectroscopy (ICP-OES at Pakistan Institute of Nuclear Science and Technology (PINSTECH), Islamabad, Pakistan.) analysis was also used to identify the trace elements. The study concluded with a geographical spatial distribution model of gold that identifies economic zones in the studied region.

The petrographic examination was carried out by producing thin sections of sediment granules for mineralogical identification by using a Lica DM 750P microscope (At the lab

of the Institute of Geology, University of Azad Jammu and Kashmir, Pakistan, in polarized light and cross nickel). Further, the opaque minerals were analyzed for the identification of heavy minerals by using a stereoscope. SEM was used to investigate the morphological characteristics and internal structures of gold grains. SEM images were used to estimate the flatness index (FI) of gold grains by comparing their length, width, and thickness. FI values were computed using the following formula: $(l + b)/2t$, where l is the length, b is the breadth, and t is the thickness of the grain [5]. It helps with the interpretation of gold deposits transported a distance from the source rock. The settings employed for the SEM analysis included an accelerating voltage of -10 kV and a counting duration of 40 s.

The elemental compositions of the samples were identified using XRF (EDX-7000 instrument at Centralized Resource Laboratory, University of Peshawar, Pakistan.) analysis. For this purpose, 10 g of pan concentrate sample was converted into powdered form. The boric jackets were produced from powdered materials, which were put in a plastic beaker and mixed with 2 cc of elvactite binding agent before drying for 15 min. The samples were placed into a steel ring (3–4 cm in diameter) to form a disk. Powdered boric acid was poured into the sample, which was subsequently compressed at 20 tons for 15–30 s. It helps in the preparation of boric jackets that have been dried for 15 min. The resulting peaks were then calibrated in order to determine the various components and their percentage composition in each sample. The X-Ray Data Booklet [36] was used to calibrate the energy (k) values as well as the photon bombardment range. The ICP-OES analysis, on the other hand, was used to determine accurate ranges of traces (including gold) and rare earth elements from different clusters, which was then used to pinpoint locations with greater potential for gold deposits. Before the study started, the following parameters were set: radio frequency generator power, 1150 W; pump rate, 50 rpm; auxiliary gas flow rate, 0.5 L min^{-1} ; and viewing plasma height, 14 mm. A scan run was originally conducted on all of the sample solutions to validate the targeted elements. For each element, three distinct analytical wavelengths were preselected. For additional quantitative investigations, the wavelength with the highest intensity, few detection limits, and low influence on the background of an emission line was selected among these. To begin the analysis, samples were also aspirated for 1 min, and the equipment was planned to generate the average values by analyzing each solution three times.

Finally, AAS was utilized to determine the quantity of gold in the studied samples. It comprises the measurement of gold in typical samples using the graphite furnace atomic absorption spectrometry technique [37,38]. The samples were finely powdered for this purpose, and 10 g of this powder was placed in a conical flask using an analytical balance. Then, aqua regia was added to the sample (mixture of HCl and HNO_3 , 3:1), for 10 min before being put on a hot plate and heated to about 80 to 90 °C. After allowing the samples to cool for 10 min, distilled water was added to dilute the solution to 50 mL. The solution was allowed to rest for a while so that the solid component could settle. The beaker's content was filtered and washed with 6N HCl to get a filtrate of 50 mL volume. The filtrate was added to a 250 mL separator funnel, followed by another 50 mL of distilled water to make the solution 100 mL. After that, 20 mL of methyl-isobutyl ketone was added, and the mixture was rolled for 8 min. After some time, the two layers were formed in the separatory funnel, with the lower layer being acidic (inorganic) and the upper layer containing gold, being methyl-isobutyl ketone. Finally, the two layers were separated from each other, and samples were analyzed on AAS, by using formula (1) through which the values of gold in ppm ($\frac{\mu\text{g}}{\text{g}}$) were calculated [39].

$$\text{ppm} \left(\frac{\mu\text{g}}{\text{g}} \right) = \frac{\text{ppm} \times V_a \times V_{(\text{MIBK})}}{\text{wt. of sample} \times V_b} \quad (1)$$

V_a = volume of the sample after dilution.

V_b = volume taken for methyl-isobutyl ketone (MIBK) extraction.

A standard sample of gold was run to ensure the precision and accuracy of the results, which are shown in the concentration and absorbance graph. The AAS plastic nebulizer

was discharged into the sample to conduct this analysis. The AAS sucked in the fluid and detected the gold concentration, displaying the results in milligrams per liter on the system associated via its software. The readings were then converted from milligrams per liter to parts per million (ppm). Following these experiments, an ArcGIS geographical distribution model was developed using AAS data. The inverse distance weighted (IDW) interpolation technique, which provides a definite result on the distribution of placer gold to find the economic potential zones in the study area, was employed for this purpose.

4. Results and Discussion

4.1. Petrographic Study

A petrographic study was carried out to determine the mineralogical composition within Indus River deposits. The microscopic features of the quartz grains mostly indicate that they are angular to subangular. The general composition indicates that the quartz ranges from 40% to 49%. The quartz grains are monocrystalline and polycrystalline (Figure 4k). Whereas monocrystalline quartz varies from 30% to 42% and polycrystalline quartz ranges from 3% to 14%. The feldspars recognized as plagioclase, orthoclase, and microcline perthite in the samples are up to 24% to 37%. Further, the rock fragments include igneous (2% to 8%), metamorphic (3% to 8%) and sedimentary (2% to 7%) clasts. These rock fragments are of different shapes, including angular to subangular. The accessory minerals (including muscovite and biotite constitute) vary from 3% to 10%, while tourmaline, hornblende, and epidote range from 3% to 7% (Table 1). The opaque minerals, on the other hand, vary from 1% to 5%. Because this study is based on clusters, the proportion of quartz in clusters C4 and C5 is slightly higher than in C1, C2, and C3, whereas clusters C1, C4, and C5 have more feldspar content than C2 and C3. Clusters C2 and C5 are enriched in igneous and sedimentary rock fragments. Cluster C2 contains slightly more metamorphic fragments than other clusters. Further, clusters C2 and C3 have relatively high accessory minerals, though clusters C1 and C2 have comparatively low opaque minerals (Figure 5).

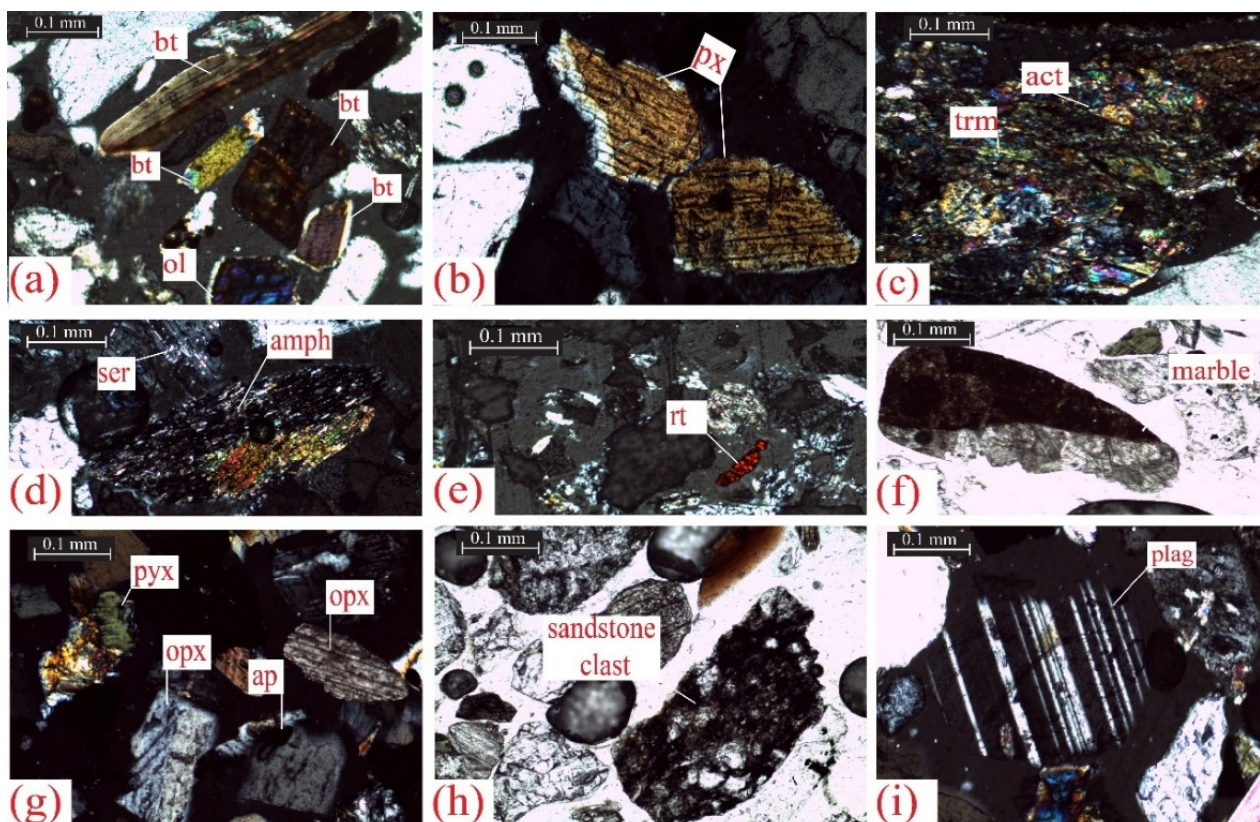


Figure 4. Cont.

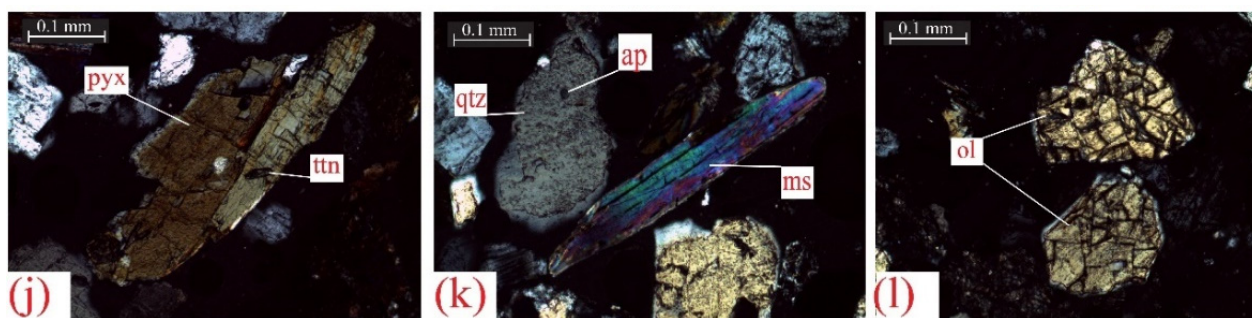


Figure 4. Microphotograph showing the average sediment composition of all the clusters (a) Biotite (bt), olivine (ol), (b) pyroxene (px), (c) actinolote (act) and tremolite (trm), (d) sericite (ser) and amphibolite (amph), (e) rutile (rt), (f) marble clast, (g) pyroxene (pyx), orthopyroxene (opx), apatite (ap), (h) sandstone clast with hematite as cementing material, (i) plagioclase (plag), (j) pyroxene (pyx) with sphene (ttn) inclusion, (k) quartz (qtz) with apatite (ap) inclusion and muscovite (ms), (l) olivine (ol) in the samples collected from the study area (scale 0.1 mm). The presence of feldspar, notably plagioclase albite and alkali feldspar, indicates a volcanic origin (Figure 4i). The alkali feldspar, on the other hand, indicates a felsic igneous origin.

Table 1. The mineralogical composition of samples in different clusters (C1, C2, C3, C4 and C5).

Mineralogical Composition		Clusters																								
		C1					C2					C3					C4					C5				
		S1	S2	S3	S4	S5	S1	S2	S3	S4	S5	S1	S2	S3	S4	S5	S1	S2	S3	S4	S5	S1	S2	S3	S4	S5
Quartz	Polycrystalline	3	5	4	5	3	12	10	11	13	13	12	13	11	14	13	9	11	10	12	11	11	12	14	11	14
	Monocrystalline	41	40	42	43	45	30	32	35	35	31	33	35	37	35	34	31	30	34	37	36	35	34	31	30	35
Feldspar		30	32	35	33	36	31	28	25	24	26	33	29	31	30	32	33	35	36	34	37	33	32	30	35	30
Rocks Fragments	Igneous	7	6	5	4	3	6	7	8	7	8	3	5	5	4	4	5	4	4	2	4	5	6	8	4	4
	Metamorphic	6	4	3	5	4	4	6	4	8	7	5	4	3	5	3	4	6	3	5	4	4	3	5	6	5
	Sedimentary	3	5	3	4	4	5	6	5	3	4	2	3	3	2	5	3	4	5	3	4	4	5	7	4	2
Accessory Minerals		4	4	6	5	3	10	9	8	7	7	9	8	5	6	4	7	5	4	3	2	6	4	3	5	6
Opaque Minerals		3	4	2	1	2	2	2	4	3	4	2	3	5	4	5	3	5	4	4	2	2	4	2	5	4
Total		100	100	100	100	100	100	100	100	100	100	100	100	100	100	100	100	100	100	100	100	100	100	100	100	

In order to investigate the unidentified mineral type in heavy minerals, opaque mineral identification was also analyzed using a stereoscope. Zircon, olivine (Figure 4l), pyroxene (Figure 4b), biotite, epidote, amphibole (Figure 4d), hornblende, and tourmaline, rutile (Figure 4c,e), and sphene (Figure 4j) were identified as heavy minerals (Table 2). The alteration of plagioclase to sericite (sericitization) is also observed (Figure 4d). Plagioclase also consists of sericite and biotite (Figure 4a), which were altered into muscovite due to sedimentary alterations.

4.2. Morphological Features of the Alluvial Gold

The gold particles picked with the stereoscope were further analyzed to understand the internal structure and transport distance of the alluvial gold particles. The morphology of gold particles from recent alluvial deposits varies according to transport distance due to internal ductile deformation [40]. It is assumed that the majority of the grains are well rounded and folded (Figure 6a,b). Their surface textures are almost smooth, elongated, and flattened (Figure 6c–f). The particle size ranges from 100 to 3000 μm. The recovered grains’ flatness index (FI) values range from 4.8 to 31.21, indicating their transit distance from a distal source in an alluvial setting (Table 3).

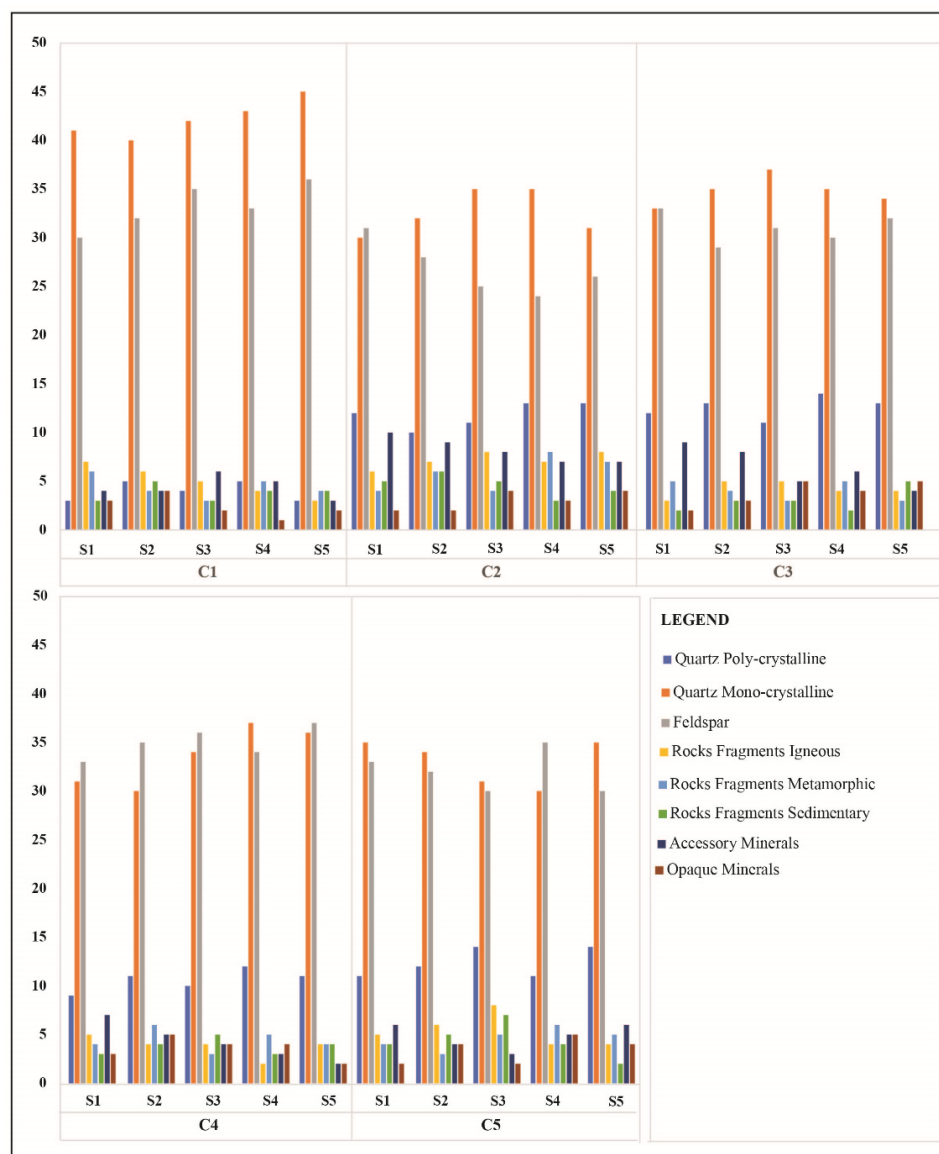


Figure 5. The mineralogical composition of Indus River deposits in samples of different clusters (C1, C2, C3, C4 and C5).

Table 2. The heavy mineral percentage of samples (HMC = weight percentage of heavy minerals, ZTR = ultrastable minerals (zircon, tourmaline, rutile), A = amphibole, Px = pyroxene, O + S = olivine + chromspirel, LgM = low-grade minerals (mostly epidote group minerals), Gt = garnet, HgM = high-grade minerals (staurolite, andalusite, kynite, silliminite and other minerals (mainly sphene).

Clusters	HMC%	ZTR	A	Px	O + S	LgM	Gt	HgM	Total
C1	3	3	53	15	5	13	8	3	100
C2	2	4	52	16	4	15	7	2	100
C3	2	2	54	12	6	17	6	3	100
C4	3	2	50	13	7	17	7	4	100
C5	2	3	52	10	10	16	6	3	100

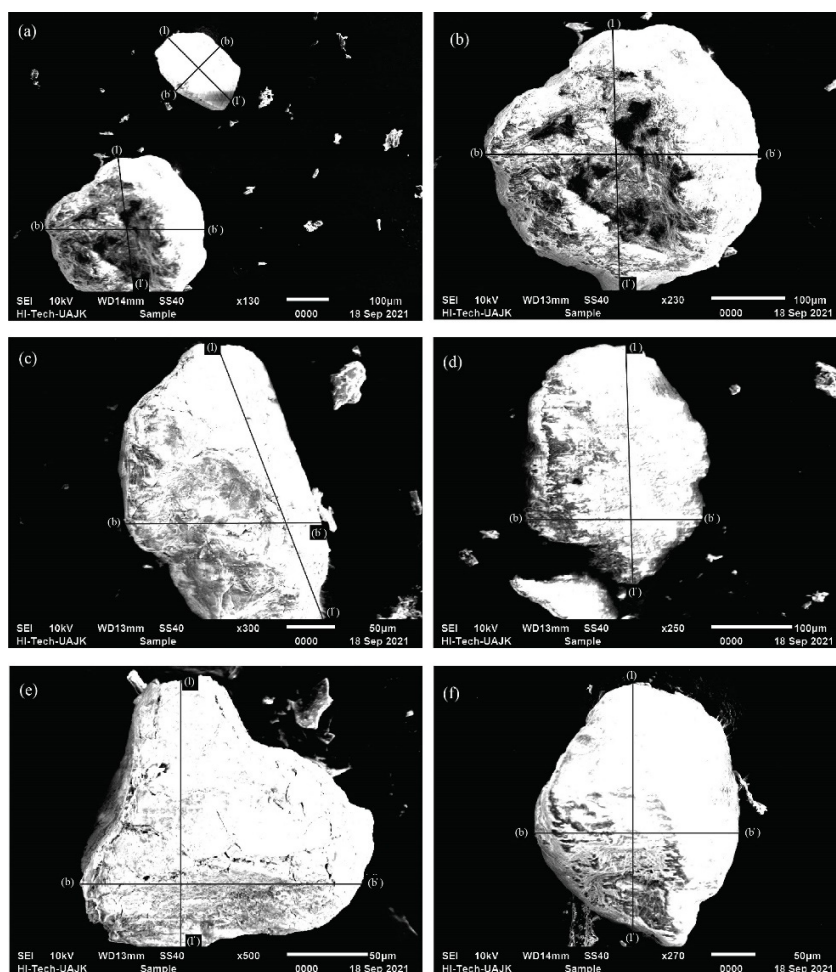


Figure 6. (a,b) SEM microphotographs interpreted as rounded gold grains affected during transport in the Indus River, whereas (c–f) indicate sub-rounded, smooth, and flattened morphology of gold grains from the study area.

Table 3. Morphological parameters include length, width, thickness, and flatness index of selected gold grains from the study area.

Cluster	Sample	Length L (Mm)	Width B (Mm)	Thickness T (Mm)	Flatness Index (FI)
C1	S1	214	143	24.665	7.2
	S2	180	110	18.8	7.7
	S3	349	361	28.782	12.33
C2	S1	344	354	16.24	21.49
	S2	213	234	14.5	4.8
	S3	309	205	30.289	8.48
C3	S1	296	245	11.773	21.829
	S2	301	206	13.97	11.20
	S3	818	606	25	28.48
C4	S1	312	221	13.76	19.36
	S2	421	167	9.42	31.21
	S3	251	144	11.65	16.95

Table 3. Cont.

Cluster	Sample	Length L (Mm)	Width B (Mm)	Thickness T (Mm)	Flatness Index (FI)
C5	S1	137	119	7.43	17.22
	S2	371	287	11.65	28.24
	S3	290	198	13	18.76

4.3. Geochemical Analysis

4.3.1. Major Element Oxides

The comparative elemental composition of alluvial sediments indicates that silica (SiO_2) is the most common constituent of sand identified in the samples as quartz. The Indus River sand has high silicon dioxide (SiO_2), iron oxide (Fe_2O_3), and aluminum oxide (Al_2O_3) contents. In addition, low levels of calcium oxide (CaO), and titanium oxide (TiO_2) were observed. Other oxide minerals identified in their composition include potassium oxide (K_2O), manganese oxide (MnO), zirconium dioxide (ZrO_2), vanadium oxide (V_2O_5), chromium oxide (Cr_2O_3), thorium dioxide (ThO_2), yttrium oxide (Y_2O_3), copper oxide (CuO), strontium oxide (SrO), zinc oxide (ZnO), and niobium oxide (NbO) (Table 4).

4.3.2. Trace and Rare Earth Elements

ICP-OES analysis was performed to identify and quantify trace and rare earth elements in representative samples of different clusters. The results indicated higher ranges of Mn, V, Ce, Cr, La, and Nd can be explored economically for industrial usage. However, elements such as Zn, Y, As, and Co were identified in lesser amounts. Precisely, gold is detected in this analysis with these trace and rare earth elements. It is observed that the clusters (C1, C2, C3) have a higher gold content value than the other clusters (C4, C5). The rare earth elements La, Ce, Nd, Yb, and Lu were also detected. La, Ce, and Nd are light rare earth elements (LREE), whereas Yb and Lu are heavy rare earth elements (HREE). The trace element and rare earth element composition of the alluvial sediments are given in Table 5.

The correlations between the detected trace element composition of the sedimentary bulk and the upper continental crust (UCC) are also evaluated [41]. As a result, trace element concentrations are influenced by weathering, provenance, sediment sorting, diagenesis, and aqueous geochemistry. The Indus sediments are considerably enriched in Au, As, Lu, Sc, Yb, and Zn and depleted in Ba, Ce, Co, Cr, La, Mn, Nd, Ni, Sc, Sr, V, and Y compared to UCC (Figure 7).

Further, the granite provenance data plots (Cr/v vs. Y/Ni) also demonstrate that these sediments come from an acidic/granitic source (Figure 8).

4.3.3. Gold Determination in Quaternary Sediments

According to the AAS analysis, the quantity of gold varies in each sample from different clusters. Overall, the results specified that the gold detection ranged from 0.34 to 13.02 ppm in the studied area. The clusters (C1, C2, C3) on the left bank of the Indus River have high values. The clusters (C4, C5) on the right bank contain a low concentration of gold. The average concentration of economic gold for exploration is greater than 5 ppm [43]. The findings show that the average value of clusters C1, C2, and C3 has a greater gold content and can be more cost-effective for exploration (Table 6).

Table 4. Overall Indus River sand composition (in weight %).

Oxides	Cluster Name									
	C1		C2		C3		C4		C5	
	Sample Names									
	S1	S2	S1	S2	S1	S2	S1	S2	S1	S2
SiO ₂	46.9	44.9	45.94	46.9	44.91	51.04	54.55	51.12	53.95	45.84
Fe ₂ O ₃	46.9	42.47	43.95	45.9	42.67	23.97	23.97	24.20	25.72	43.96
Al ₂ O ₃	12.6	14.64	13.62	12.6	14.24	11.74	10.98	12.23	11.82	13.61
CaO	6.1	5.19	7.12	6.11	8.19	6.52	6.52	7.43	8.21	7.22
TiO ₂	4.4	3.50	4.01	4.42	3.53	4.36	4.36	5.54	8.68	4.01
K ₂ O	0.8	0.56	0.80	0.84	0.46	1.21	1.22	2.00	1.10	0.82
MnO	0.61	0.70	0.61	0.61	0.79	0.39	0.44	0.50	0.45	0.64
ZrO ₂	0.41	0.42	0.42	0.41	0.48	0.29	0.45	0.39	0.78	0.45
V ₂ O ₅	0.16	0.15	0.18	0.19	0.13	0.20	0.11	0.10	0.87	0.18
Cr ₂ O ₃	0.14	0.19	0.14	0.12	0.12	0.17	0.19	0.19	0.16	0.15
ThO ₂	0.03	0.01	0.01	0.02	0.01	-	0.00	-	-	0.00
Y ₂ O ₃	0.02	0.01	0.02	0.02	0.01	0.01	0.01	0.00	0.02	0.03
CuO	0.01	0.06	0.01	0.01	0.06	0.01	0.01	0.05	0.01	0.02
SrO	0.01	0.01	0.01	0.01	0.02	0.02	0.01	0.02	0.00	0.01
ZnO	0.01	0.01	0.02	0.01	0.00	0.01	0.01	0.01	0.03	0.02
NbO	0.01	0.01	0.02	0.00	0.00	0.00	0.00	0.01	0.00	0.04

Table 5. Trace element concentration in the different samples of each cluster.

Clusters	C1					C2					C3					C4					C5				
	S-1	S-2	S-3	S-4	S-5	S-1	S-2	S-3	S-4	S-5	S-1	S-2	S-3	S-4	S-5	S-1	S-2	S-3	S-4	S-5	S-1	S-2	S-3	S-4	S-5
Au (ug/g)	10	7.8	8.0	11	13	9.8	6.9	7	4.3	5.68	9.80	5.87	5	3.67	3.890	4.00	2.4	3.90	2.76	4.72	1	5.32	4.90	2.90	1.68
As (ug/g)	85	85	82	80	85	83	82	84	85	88.9	80.0	80.1	82	88.1	85.32	90.1	90	89.0	92.6	90.1	89	90.9	95.8	98.30	96.70
Ba (ug/g)	41	42	43	43	42	46	45	44	41	42.1	44.3	42.3	43	45.1	41.29	50.0	47	49.5	48.7	49.5	48	50.7	55.9	52.30	51.54
Ce (ug/g)	438	458	438	397	458	403	40	402	438	428	387	381	361	380	438.1	432	453	444	438	453	369	365	370	350.5	366
Co (ug/g)	58	68	72	60	68	59	59	56	53	51.2	60.1	59.8	61	63.7	53.35	56.4	56	54.7	53.6	56.7	49	47.8	51.2	55.65	58.54
Cr (ug/g)	372	388	372	369	388	321	324	324	372	382	354	358	349	351	382	323	319	322	318	322	398	355	375	371.30	380.87
La (ug/g)	286	246	286	288	216	263	243	233	245	265	278	282	277	286	235	276	271	273	250.5	252.3	289	280	282	277.6	276.4
Lu (ug/g)	9.8	10	9	10	10	9	9	9	9.5	9.98	10.0	9.80	11	11.5	9.870	8.92	8.9	9.06	9.06	7.99	9.76	10.0	10	9.550	8.990
Mn (ug/g)	3444	3564	3246	3674	3565	3827	3628	3598	3664	3704	3674	3682	3699	3490	3674	3564	355	3499	3199	3276	3789	3770	3754	3720	3749
Nd (ug/g)	262	232	252	221	22	232	212	220	242	244	221	225	221	225	282	202	202	205	199	200	254	260	258	265.6	278.8

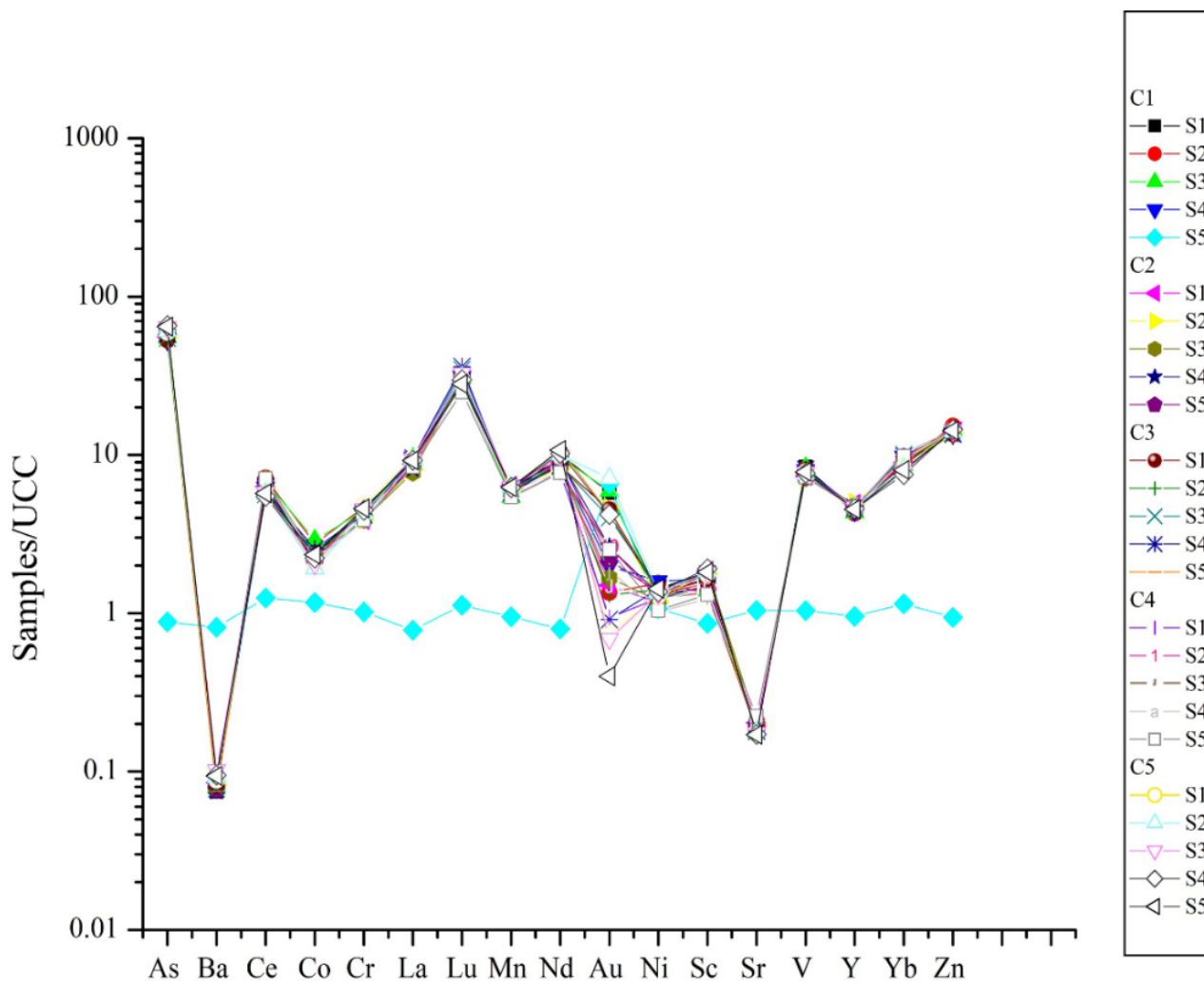


Figure 7. Trace element diagram for the sediments of the Indus River. After UCC standard [41], a graph shows the high values of Au, As, Lu, Sc, Yb, Z in the samples. Sample C1-S5 indicates high gold concentration and low concentration of other elements, which may be due to the hydrothermal quartz vein that contains gold.

Further, the gold spatial distribution model was developed using the results of the AAS analysis (Figure 9). According to the spatial distribution of gold, the southeastern half (C1) of the studied area has significant concentrations of gold deposits, although the C2 and C3 on the same side of the river had AAS values of more than 10 ppm gold. C4 and C5 have the lowest gold concentrations.

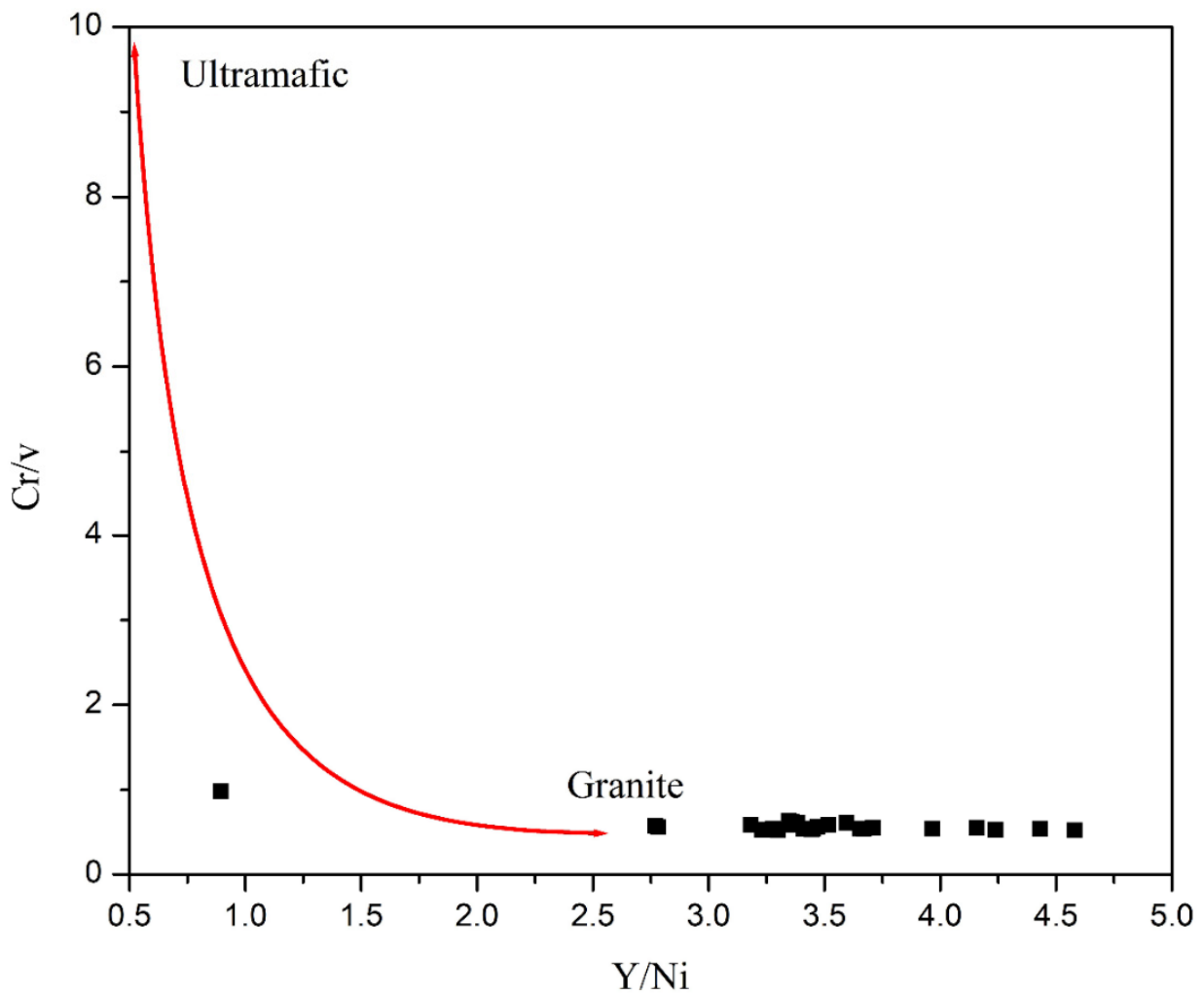


Figure 8. Provenance discrimination diagrams. Cr/V vs. Y/Ni after [42], sample plot in granitic source showing the granitic provenance of sediments.

Table 6. Gold concentrations in pan concentrate samples of the study area.

Cluster	Sample Name	GOLD (ppm)	Average (ppm)
C1	S1	11.4	10.406
	S2	9.8	
	S3	7.58	
	S4	10.23	
	S5	13.02	
C2	S1	10.2	6.93
	S2	8.9	
	S3	7.3	
	S4	5.04	
	S5	3.21	

Table 6. Cont.

Cluster	Sample Name	GOLD (ppm)	Average (ppm)
C3	S1	8.01	4.982
	S2	6.2	
	S3	3.4	
	S4	4.9	
	S5	2.4	
C4	S1	3.9	2.452
	S2	1.34	
	S3	1.9	
	S4	2.02	
	S5	3.1	
C5	S1	0.34	2.768
	S2	5.93	
	S3	1.34	
	S4	2.45	
	S5	3.78	

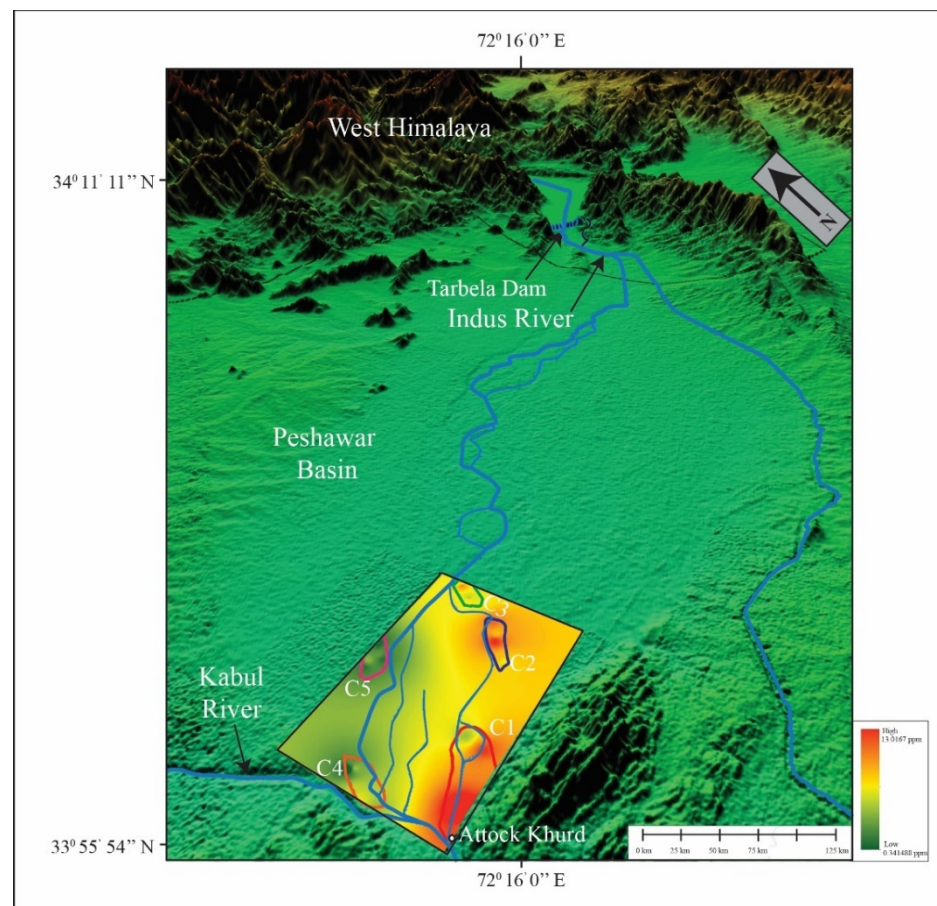


Figure 9. A model based on quantitative gold distribution showing the high- and low-concentration zones of gold (ppm) in the study area deposited through the Indus River from Himalaya.

5. Discussions

Petrographic studies of river sediments were carried out to determine the origin of these sediments. The petrographic investigation revealed that the detected quartz is mostly angular, subangular, and rounded in shape. It was observed in all of the clusters, suggesting a mixed Himalayan origin. It also suggests that the sediments were mostly composed of epidote, sericite, tourmaline, zircon, and actinolite. Epidote is derived from greenschists or formed by hydrothermal alteration, while sericite is a fine-grained white mica formed by feldspar alteration. In felsic igneous rocks, pegmatites, and metamorphic rocks, tourmaline is formed (granet gneiss). Zircon may be identified in three types of rocks: igneous, metamorphic, and sedimentary. Actinolite indicates that it was metamorphosed from Himalayan mafic and ultramafic rocks. The lithic fragments are composed of volcanic (Figure 3f), metamorphic, and sedimentary rocks, indicating a diverse source of Himalayan sediments. The mineral assemblage suggests that these sediments were derived from plutonic, volcanic basic, and ultrabasic rocks. Certain mineral assemblages, on the other hand, indicate the origin of metamorphic and sedimentary rocks.

In the QFL diagram [44], the modal compositional data of the alluvial sediments were plotted on the recycled orogen provenance field that occurred in the Himalaya (Figure 10a,b), where igneous, metamorphic, and sedimentary rocks were deformed and uplifted due to the ongoing Himalayan Orogeny, and these sediments were transported by active fluvial systems, where finally this detritus (also including gold grains and other heavy minerals) was deposited where the velocity of water sufficiently dropped. It is believed that the Indus River contains a rich amount of sediment from the Karakorum and Hindukush regions. The sediments of the Hunza River originate from the Ladakh and Kohistan tributaries. Further, the Shyok and Astor rivers (originating in the Deosai Mountains) and the Gilgit River (originating in the Gilgit Complex) are depositing sediments from Himalayan tributaries through the Indus River.

According to the morphological study, the samples mostly consist of microscopic flaky gold grains. The roundness, flatness, flakiness, and smallness are all related to a spongy surface appearance. It indicates that gold grains have traveled a long distance from the source through the active fluvial system of the Himalaya. It is interpreted that the high-energy fluvial system with a sharp slope often contains placer deposits that are occasionally altered. The Ako'ozam and Njabilobe are river streams in the southwestern Cameroon range that also transport gold grains through an active fluvial system. The gold grains recovered from the Indus sediments range from 100 to 3000 μm , whereas the gold particles of the Ako'ozam and Njabilobe stream placers range from 50 to $>600\mu\text{m}$ [45]. In both cases, the gold grains have a sub-rounded, elongated, and folded shape. The Ako'ozam and Njabilobe gold particles, on the other hand, were transported from a nearby source, while the Indus gold particles were transported from a distal source.

The elemental composition of the sediments is a very powerful tool in provenance analysis. The Fe_2O_3 is thought to have been derived from hematite, limonites, and magnetite. The CaO and TiO_2 originated from limestone and either rutile or sphene, respectively. Titanite (sphene) is therefore an accessory mineral in I-type granites as well as formed in metamorphosed rocks. This shows the presence of I-type granites and metamorphosed rocks in the source. As a result, intrusion-related gold systems are associated with I-type granites [46]. The Amani River in Tanzania also transports gold grains through fluvial systems. As a comparison between the geochemical characteristics of these rivers, it is interpreted that these characteristics are similar in both rivers, as both rivers have a high SiO_2 content. The Amani River, on the other hand, has a wide range of silica concentration (45% to 75%) owing to acidic and alkaline rocks, but the Indus River has a narrow range [41]. Similarly, the least abundant oxides in Amani River sediments are Cr_2O_3 , CaO, MnO, MgO, Na_2O , and P_2O_5 , each accounting for <1 wt.%. The Indus River, on the other hand, has a high concentration of Fe_2O_3 , Al_2O_3 , CaO and TiO_2 (<10 wt.%), whereas the least abundant oxides are K_2O , MnO, ZrO_2 , V_2O_5 , Cr_2O_3 , ThO_2 , Y_2O_3 , CuO, SrO, ZnO and NbO which are <1 wt.%.

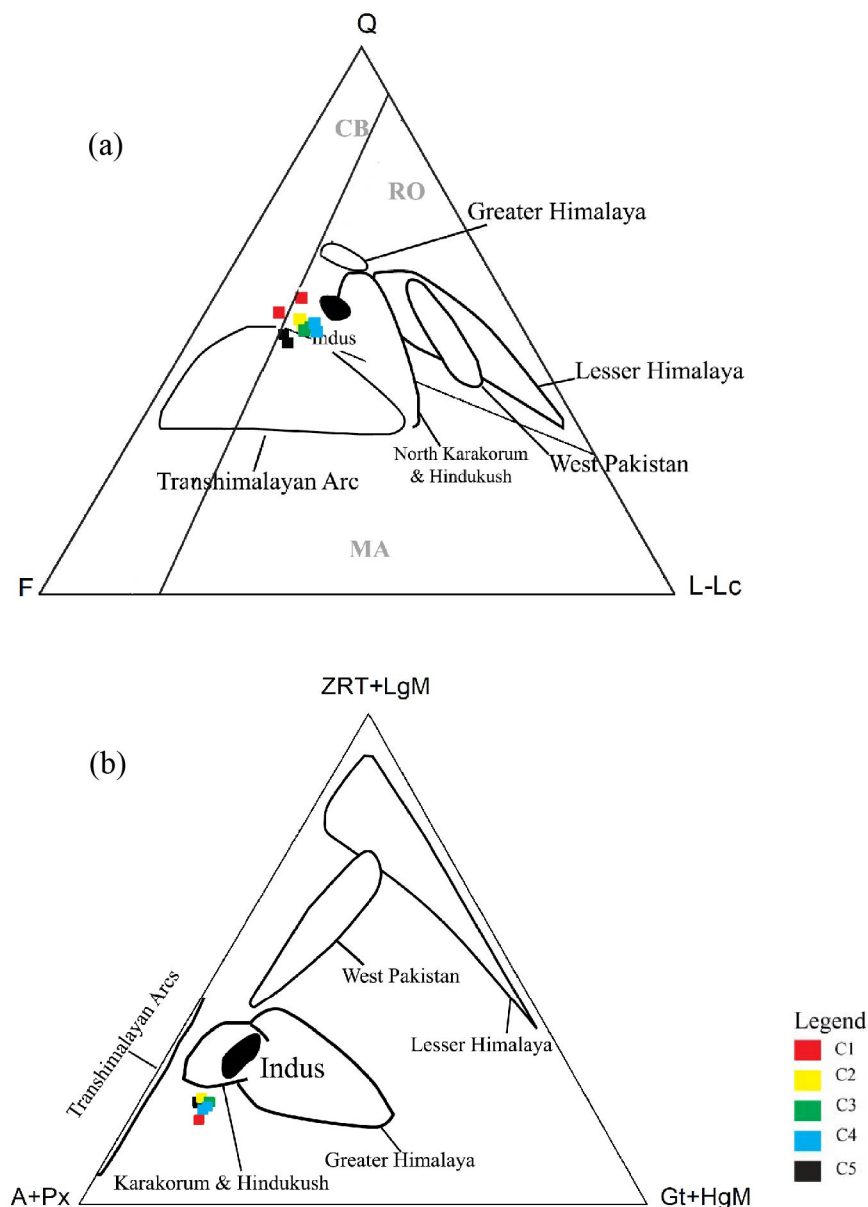


Figure 10. The triangular plots show (a) petrography, Q = quartz, F = feldspar, L-Lc = lithic-lithics carbonates and (b) heavy-mineral assemblages, ZRT + LgM = ultrastable minerals zircon tourmaline rutile + low grade minerals mostly epidote group minerals, A + Px = amphibole + pyroxene, Gt + HgM = garnet + high-grade minerals mainly sphene, carried by the Indus River plot near the boundary between recycled orogen (RO), magmatic arc (MA), and continental block (CB) provenance fields [44].

The concentration of trace and rare earth elements in alluvial sediments is another crucial factor in determining their origin. There is an enrichment of LREE in the studied alluvial sediments compared to HREE, suggesting that these sediments originated from crustal rocks. The presence of hornblende, garnet, sphene, and pyroxene in these sediments likely contributed to the presence of rare earth elements (Table 2). The results presented on the provenance discrimination diagram Cr/V vs. Y/Ni confirm the river sediments' granitic origin. Minor minerals of I-type granites that include porphyry copper, tungsten, and molybdenum deposits include hornblende, sphene, and pyroxene. In addition to copper deposits, porphyry copper deposits contain gold. By comparison, the trace elements associated with gold identified in the Amani River sediments are believed to have

essentially identical concentrations of As, Co, Cr, Mn, Ni, Se, Sr, V, and Zn to those reported in the Indus deposits [47].

According to AAS analysis and spatial distribution of river sediments, there is a high concentration of gold on the left bank of the river compared to the right bank of the river. The reason is that the left side of the river has more potential for gold exploration due to low water velocity in point bars and channel bars of the river (Figure 9). Hence, the rivers have two banks. On one bank, it erodes the sediments due to its high velocity, while on the other bank, it deposits the sediments due to its low velocity. The deposition occurs where the velocity sufficiently drops. In the study area, the channel bars were located on the left bank of the river, which deposited the sediments opposite to the erosional bank.

The Indus River passes through the KIA, which is composed of ultramafic and mafic rocks with very unstable high-temperature minerals. These minerals were not identified in the samples, suggesting that they were weathered during transportation.

6. Conclusions

Based on the petrographic, SEM, and geochemical investigations, the following conclusions are drawn.

According to petrographic studies, the Indus River sediments (which include heavy minerals) are transported from the Himalaya's deformed and uplifted rocks, which are composed of igneous (plutonic and volcanic basic and ultrabasic rock origins) and metamorphic rocks. The mixed source of sediment deposition is also indicated by the elemental composition. The presence of high concentrations of silicon dioxide, iron oxide, and aluminum oxide has been identified. The petrographic investigation also reveals the presence of hornblende, pyroxene, and sphene, which are minor minerals observed in I-type granites. porphyry Cu, Mo, and W deposits are identified in I-type granite. Gold is detected as a byproduct in porphyry Cu deposits. It is determined that these alluvial deposits are mostly the result of weathering and erosion of I-type granites. The trace elements show that the sedimentary bulk in the study area is quite enriched in Au, As, Lu, Sc, Yb, and Zn. The provenance discrimination plotted using geochemical data reveals that both sediments originated from the same granitic source. According to the SEM analysis, the gold grains have a high flatness index and are well rounded and folded. Their surface texture is partially smooth, elongated, and flattened, suggesting a transportation of more than 100 km. The AAS analysis summarizes the feasible areas (C1, C2, and C3) for further investigation of gold deposit economic potential. According to the study, clusters C1, C2, and C3 have higher gold concentrations owing to low water velocity caused by channel bars and point bars compared to clusters C4 and C5, which have a relatively high running-water velocity.

The spatial distribution model reveals that the left riverbank of the studied area has a high concentration of gold resources that may have greater potential for commercial gold exploration than the right riverbank. Overall, the analysis reveals that the research region has high potential for commercially exploiting gold reserves.

Author Contributions: Conceptualization, A.W. and A.M.; methodology, A.W.; software, A.W.; validation, M.S.M., H.T.J. and A.W.; formal analysis, A.W., M.A.S. and H.T.J.; investigation, A.W. and S.H.A.; resources, A.W. and N.A.S.; data curation, A.W. and A.M.; writing—original draft preparation, A.W., H.T.J. and S.H.A.; writing—review and editing, A.W., H.T.J., G.K., O.K. and N.A.S.; visualization, A.W. and M.A.S.; supervision, A.W.; project administration, A.W. and H.T.J.; funding acquisition, A.W., O.K., G.K. All authors have read and agreed to the published version of the manuscript.

Funding: This research received no external funding.

Data Availability Statement: Not applicable.

Acknowledgments: We are thankful to the Institute of Geology and Centralized Resource Laboratory, University of Azad Jammu and Kashmir for the petrographic and SEM analysis, respectively. We are also grateful to the Centralized Resources Lab, University of Peshawar, and Central Analytical Facility Division (CAFD), Pakistan Institute of Nuclear Sciences and Technology (PINSTECH), Islamabad for their support in sample analysis.

Conflicts of Interest: The authors declare no conflict of interest.

References

1. Kirk, J.; Ruiz, J.; Chesley, J.; Tittley, S. The Origin of Gold in South Africa. *Am. Sci.* **2003**, *91*, 534. [[CrossRef](#)]
2. Pan, B.; Pang, H.; Gao, H.; Garzanti, E.; Zou, Y.; Liu, X.; Li, F.; Jia, Y. Heavy-mineral analysis and provenance of Yellow River sediments around the China Loess Plateau. *J. Asian Earth Sci.* **2016**, *127*, 1–11. [[CrossRef](#)]
3. Vikent'eva, O.V.; Prokofiev, V.Y.; Gamyarin, G.N.; Goryachev, N.A.; Bortnikov, N.S. Intrusion-related gold-bismuth deposits of North-East Russia: PTX parameters and sources of hydrothermal fluids. *Ore Geol. Rev.* **2018**, *102*, 240–259. [[CrossRef](#)]
4. Nikiforova, Z. Criteria for Determining the Genesis of Placers and Their Different Sources Based on the Morphological Features of Placer Gold. *Minerals* **2021**, *11*, 381. [[CrossRef](#)]
5. Ali, A.; Rehman, K.; Tayyab, O.; Zaman, T.; Jameel, M.; Khan, A.; Ahmad, R.; Irfan, M. Exploring Placer Gold Deposits through Integrated Geophysical and Geochemical Techniques at the Confluence of the Indus and Kabul Rivers, NW Pakistan. *Acta Geol. Sin.-Engl. Ed.* **2020**, *94*, 1440–1450. [[CrossRef](#)]
6. Prasad, U. *Economic Geology Economic Mineral Deposits*, 2nd ed.; CBS Publishers & Distributors Private Ltd: Delhi, India, 2012.
7. Dill, H.G. Gems and placers—A genetic relationship par excellence. *Minerals* **2018**, *8*, 470.
8. Rashid, N.; Zafar, M.; Ahmad, M.; Malik, K.; Shah, S.N.; Sultana, S.; Zahid, N.; Noshad, Q.; Siddiq, Z. Use of scanning electron microscopy to analyze sculpturing pattern and internal features of pollen grain wall in some members of Astragaleae (subfamily: Papilionoideae). *Microsc. Res. Tech.* **2022**, *85*, 1631–1642. [[CrossRef](#)]
9. Alam, M.; Li, S.R.; Santosh, M.; Yuan, M.W. Morphology and chemistry of placer gold in the Bagrote and Dainter streams, northern Pakistan: Implications for provenance and exploration. *Geol. J.* **2019**, *54*, 1672–1687. [[CrossRef](#)]
10. Ali, L.; Chapman, R.; Farhan, M.; Shah, M.T.; Khattak, S.A.; Ali, A. Exploration Methodology Using Morphology and Alloy Composition of Alluvial Gold: A Case Study from Quaternary Deposits of the Nowshera District, Khyber Pakhtunkhwa, Pakistan. *Min. Metall. Explor.* **2021**, *38*, 367–377.
11. Lalomov, A.; Chefranov, R.; Naumov, V.; Naumova, O.; LeBarge, W.; Dilly, R. Typomorphic features of placer gold of Vagran cluster (the Northern Urals) and search indicators for primary bedrock gold deposits. *Ore Geol. Rev.* **2017**, *85*, 321–335. [[CrossRef](#)]
12. Youngson, J.; Craw, D. Gold nugget growth during tectonically induced sedimentary recycling, Otago, New Zealand. *Sediment. Geol.* **1993**, *84*, 71–88. [[CrossRef](#)]
13. Omang, B.; Suh, C.; Lehmann, B.; Vishiti, A.; Chombong, N.; Fon, A.; Egbe, J.; Shemang, E. Microchemical signature of alluvial gold from two contrasting terrains in Cameroon. *J. Afr. Earth Sci.* **2015**, *112*, 1–14. [[CrossRef](#)]
14. Ali, L.; Moon, C.J.; Williamson, B.J.; Shah, M.T.; Khattak, S.A. A GIS-based stream sediment geochemical model for gold and base metal exploration in remote areas of northern Pakistan. *Arab. J. Geosci.* **2015**, *8*, 5081–5093. [[CrossRef](#)]
15. Miandad, S.; Shah, M.T.; Khan, S.D.; Ahmad, L. Investigation for gold and base metals mineralization and petrochemical characteristics of the rocks of upper parts of Bagrot valley, Gilgit-Baltistan, Pakistan. *J. Himal. Earth Sci.* **2014**, *47*, 29.
16. Shah, M.T.; Khan, S.D.; Ahmad, L. Investigation of gold and base metals mineralization and the petrochemical studies of the associated host rocks, Shagari Bala area, Skardu Gilgit-Baltistan, Pakistan. *J. Himal. Earth Sci.* **2015**, *48*, 26–40.
17. Sheikh, L.; Shah, M.T.; Khan, S.D.; Ahmad, L. Investigation for gold and base metals mineralization and petrochemical characteristics of the rocks of Golo Das and surrounding areas, District Ghizar, Gilgit-Baltistan, Pakistan. *J. Himal. Earth Sci.* **2014**, *47*, 15–27.
18. Ghazi, S.; Ali, S.H.; Sahraeyan, M.; Hanif, T. An overview of tectonosedimentary framework of the Salt Range, northwestern Himalayan fold and thrust belt, Pakistan. *Arab. J. Geosci.* **2015**, *8*, 1635–1651. [[CrossRef](#)]
19. Bibi, M.; Wagreich, M.; Iqbal, S.; Jan, I.U. Regional sediment sources versus the Indus River system: The Plio-Pleistocene of the Peshawar basin (NW-Pakistan). *Sediment. Geol.* **2019**, *389*, 26–41. [[CrossRef](#)]
20. Bibi, M.; Wagreich, M.; Iqbal, S.; Gier, S.; Jan, I.U. Sedimentation and glaciations during the Pleistocene: Palaeoclimate reconstruction in the Peshawar Basin, Pakistan. *Geol. J.* **2020**, *55*, 671–693. [[CrossRef](#)]
21. Ghazi, S.; Ali, S.H.; Shahzad, T.; Ahmed, N.; Khalid, P.; Akram, S.; Ali, S.; Sami, J. Sedimentary, structural and salt tectonic evolution of Karoli-Nilawahana area, Central Salt Range and its impact for the Potwar Province. *Himal. Geol.* **2020**, *41*, 145–156.
22. Searle, M.P.; Treloar, P.J. London, Special Publications. Introduction to Himalayan tectonics: A modern synthesis. *Geol. Soc. London Spéc. Publ.* **2019**, *483*, 1–17. [[CrossRef](#)]
23. Yasin, Q.; Baklouti, S.; Khalid, P.; Ali, S.H.; Boateng, C.D.; Du, Q. Evaluation of shale gas reservoirs in complex structural enclosures: A case study from Patala Formation in the Kohat-Potwar Plateau, Pakistan. *J. Pet. Sci. Eng.* **2021**, *198*, 108225. [[CrossRef](#)]

24. Javed, A.; Wahid, A.; Mughal, M.S.; Khan, M.S.; Qammar, R.S.; Ali, S.H.; Siddiqui, N.A.; Iqbal, M.A. Geological and petrographic investigations of the Miocene Molasse deposits in Sub-Himalayas, District Sudhnati, Pakistan. *Arab. J. Geosci.* **2021**, *14*, 1517. [[CrossRef](#)]
25. Ashraf, M.; Dawood, H. Geology of Acid and Alkalic Minor Bodies Associated with Granitic and Alkalic Complexes of Malakand Division. *Geol. Bull. Punjab Univ.* **2010**, *45*, 49–68.
26. Ali, L.; Ahmad, S.; Khattak, S.A.; Anjum, N.; Waseem, M.; Ali, A. Economic Evaluation of Placer Gold Along River Indus From Ghazi to Kund, Khyber Pakhtunkhwa, Pakistan: Implications for Commercial Scale Pilot Plant. *Int. J. Econ. Environ. Geol.* **2019**, *10*, 129–134.
27. Wahid, A.; Rauf, A.; Ali, S.H.; Khan, J.; Iqbal, M.A.; Haseeb, A. Impact of complex tectonics on the development of geo-pressured zones: A case study from petroliferous Sub-Himalayan Basin, Pakistan. *Geopersia* **2021**, *12*, 89–106.
28. Burbank, D.W.; Tahirkheli, R.A.K. The magnetostratigraphy, fission-track dating, and stratigraphic evolution of the Peshawar intermontane basin, northern Pakistan. *Geol. Soc. Am. Bull.* **1985**, *96*, 539–552. [[CrossRef](#)]
29. Mallik, T.; Vasudevan, V.; Verghese, P.; Machado, T. The black sand placer deposits of Kerala beach, southwest India. *Mar. Geol.* **1987**, *77*, 129–150. [[CrossRef](#)]
30. Evans, A.M. *Ore Geology and Industrial Minerals: An Introduction*; John Wiley & Sons: Hoboken, NJ, USA, 2009.
31. Ahmed, N.; Ali, S.H.; Ahmad, M.; Khalid, P.; Ahmad, B.; Akram, M.S.; Farooq, S.; Din, Z.U. Subsurface Structural Investigation Based on Seismic Data of the North-Eastern Potwar Basin, Pakistan. *Indian J. Geo-Mar. Sci.* **2022**, *49*, 1258–1268.
32. Zada, K.; Arif, M.; Sajid, M.J.G. Controls and Implications of Geo-Technical Variation in Quartzose Rocks from Peshawar Basin, North-Western Pakistan. *Geomaterials* **2015**, *5*, 85. [[CrossRef](#)]
33. Hussain, A.; Pogue, K.; Khan, S.R.; Ahmad, I. Paleozoic stratigraphy of the Peshawar basin, Pakistan. *Geol. Bull. Univ. Peshawar* **1991**, *24*, 85–97.
34. Cornwell, K. Quaternary break-out flood sediments in the Peshawar basin of northern Pakistan. *Geomorphology* **1998**, *25*, 225–248. [[CrossRef](#)]
35. Ali, L.; Williamson, B.J.; Moon, C.J.; Shah, M.T.; Khattak, S.A. Distribution of gold in different size fractions of stream sediments as a guide to bedrock gold mineralisation along the Shyok Suture Zone and adjacent areas of the Kohistan Island Arc, Pakistan. *Arab. J. Geosci.* **2015**, *8*, 2227–2235. [[CrossRef](#)]
36. Thompson, A.C.; Vaughan, D. *X-ray Data Booklet*; Lawrence Berkeley National Laboratory, University of California Berkeley: Berkeley, CA, USA, 2001; Volume 8.
37. Hubert, A.E.; Chao, T.T. Determination of gold, indium, tellurium and thallium in the same sample digest of geological materials by atomic-absorption spectroscopy and two-step solvent extraction. *Talanta* **1985**, *32*, 568–570. [[CrossRef](#)]
38. Dobrowolski, R.; Mróz, A.; Dąbrowska, M.; Olszański, P. Solid sampling high-resolution continuum source graphite furnace atomic absorption spectrometry for gold determination in geological samples after preconcentration onto carbon nanotubes. *Spectrochim. Acta Part B At. Spectrosc.* **2017**, *132*, 13–18. [[CrossRef](#)]
39. Moghaddam, F.H.; Taher, M.A.; Behzadi, M.; Naghizadeh, M. Modified carbon nanotubes as a sorbent for solid-phase extraction of gold, and its determination by graphite furnace atomic absorption spectrometry. *Microchim. Acta* **2015**, *182*, 2123–2129. [[CrossRef](#)]
40. Santosh, M.; Omana, P.K. Very high purity gold form lateritic weathering profiles of Nilambur, southern India. *Geology* **1991**, *19*, 746–749. [[CrossRef](#)]
41. McLennan, S.M. Relationships between the trace element composition of sedimentary rocks and upper continental crust. *Geochem. Geophys. Geosystems* **2001**, *2*. [[CrossRef](#)]
42. Mongelli, G.; Critelli, S.; Perri, F.; Sonnino, M.; Perrone, V. Sedimentary recycling, provenance and paleoweathering from chemistry and mineralogy of Mesozoic continental redbed mudrocks, Peloritani Mountains, Southern Italy. *Geochem. J.* **2006**, *40*, 197–209. [[CrossRef](#)]
43. Baurens, S. Valuation of metals and mining companies. In *Immobilienwirtschaft Aktuell*; University of Zurich: Zurich, Switzerland, 2010.
44. Garzanti, E.; Vezzoli, G.; Andò, S.; Paparella, P.; Clift, P.D. Petrology of Indus River sands: A key to interpret erosion history of the Western Himalayan Syntaxis. *Earth Planet. Sci. Lett.* **2005**, *229*, 287–302. [[CrossRef](#)]
45. Fuanya, C.; Bolarinwa, A.T.; Kankeu, B.; Yongue, R.F.; Ngatcha, R.B.; Tangko, T.E. Morphological and chemical assessment of alluvial gold grains from Ako'ozam and Njabilobe, southwestern Cameroon. *J. Afr. Earth Sci.* **2019**, *154*, 111–119. [[CrossRef](#)]
46. Yang, X.-M.; Lentz, D.R.; Chi, G.; Thorne, K.G. Geochemical characteristics of gold-related granitoids in southwestern New Brunswick, Canada. *Lithos* **2008**, *104*, 355–377. [[CrossRef](#)]
47. Dunn, S.C.; Bjorn, P.; Rozendaal, A.; Taljaard, R. Secondary gold mineralization in the Amani placer gold deposit, Tanzania. *Ore Geol. Rev.* **2019**, *107*, 87–107. [[CrossRef](#)]